

# High spectral resolution does not aid in modeling star formation histories

L.E. Abramson<sup>1</sup>★, D.D. Kelson<sup>1</sup>, and A. Dressler<sup>1</sup>

<sup>1</sup> *Carnegie Observatories, 813 Santa Barbara Street, Pasadena, CA 91101, USA*

Accepted XXX. Received YYY; in original form ZZZ

## ABSTRACT

We compare actual  $R \sim 800$  spectroscopy to predictions generated from galaxy star formation histories (SFHs) inferred from  $R \sim 25$  rest-optical prism spectra and *ugrizJK<sub>s</sub>* photometry. Based on XXX systems with characteristics we find a median difference of  $\leq 1\%$  between all predicted and measured Lick absorption features except the Balmer lines—explainable by unmodeled emission—and Ca4227 in passive galaxies, which is up to 2.5% weaker than expected. These results hold using SFH models incorporating either five age bins, or over a hundred. Absent a Ca-age prior accurate to  $\sim 2\%$ , and provided a sufficient wavelength baseline has already been sampled, we therefore see no utility in adding high resolution spectroscopy as a flux-related constraint in SFH modeling. Our results cast doubt on the extent to which spectra from the *James Webb Space Telescope* will enhance our understanding of galaxy growth, such that progress requires new tactics more than new data.

**Key words:** galaxies: spectroscopy — galaxies: evolution

## 1 INTRODUCTION

A central ambition of the study of galaxy evolution is to understand stellar mass growth; i.e., star formation histories (SFHs). Spectral energy distributions (SEDs) are the key empirical anchor in this work because they can be decomposed into combinations of distinct stellar populations of known ages. The resulting coefficients encode the stellar mass a galaxy formed at the lookback time corresponding to each population’s age.

Different stellar populations have different but not orthogonal SEDs. Thus, galaxy SED decompositions and the SFHs inferred therefrom are degenerate (Cid Fernandes et al. 2005). The degeneracies are compounded by formally age-independent effects like metallicity and dust.

In theory, using higher resolution spectra should ameliorate this issue: the absorption lines visible in such data increase the contrast between stellar subpopulations, constrain metallicities, and so yield better age/mass coefficients. In practice, this seems unlikely.

We perform a simple experiment to assess the added utility of  $R \sim 800$  optical spectra in reconstructing SFHs as compared to  $R \sim 25$  optical prism data and broadband UV–IR photometry. We:

- (i) infer SFHs from low resolution data;
- (ii) create high resolution model spectra from those inferences;

(iii) compare the predictions to high resolution data obtained post facto for the same objects.

In a sample of XXX galaxies at  $\langle z \rangle = \text{ZZZ}$ , we predict all but one Lick absorption feature (Worthey 1994) to better than 1% in the median—including those outside the original prism band-pass. The exception—Ca4227 in passive galaxies only—is known to behave anomalously, and is only  $\sim 2.5\%$  weaker than expected.

We conclude that the additional pixels in high resolution spectra do not add meaningful flux-related SED constraints for individual galaxies compared to much more coarsely but broadly sampled data. As such, we suggest future surveys aimed at supporting SFH reconstruction opt for wavelength coverage over spectral resolution in their designs.

Section 2 describes the data for our experiment. Section 3 compares the spectral predictions to the high resolution data; 3.2 contains our key results. Section 4 discusses implications. We use AB magnitudes and assume a Chabrier (2003) stellar initial mass function (IMF) with  $(H_0, \Omega_M, \Omega_\Lambda) = (70 \text{ km s}^{-1} \text{ Mpc}^{-1}, 0.3, 0.7)$  throughout.

## 2 DATA

### 2.1 Master sample

We use data from the *Carnegie Spitzer IMACS Survey* (CSI; Kelson et al. 2014). CSI provides Magellan-IMACS Low- and Uniform-

★ E-mail: labramson@carnegiescience.edu

Dispersion Prism spectroscopy (CITE) for objects with *Spitzer* [3.5]  $\leq 21$  in **XXX sq. deg.** from **THESE FIELDS**. Combined with supplemental *ugrizJKs* photometry from the NEWFIRM archive (CITE) and Canada-France-Hawai'i Telescope Legacy Survey (CFHTLS; CITE), these data were used to derive flexible SFHs for each galaxy during redshift estimation. The sample is unbiased to  $\log M_*/M_\odot \sim 10.3$  at  $z \sim 0.7$ . The spectral resolution of the prisms varies from  $R \sim \text{XXX}$  to  $R \sim \text{YYY}$  at **wavelengths**, about **80×** coarser than the Sloan Digital Sky Survey (York et al. 2000).

We derive SFHs from these data in two ways. Our results are quantitatively similar using either approach.

### 2.1.1 Technique 1 for inferring SFHs from low resolution SEDs

The CSI spectrophotometry was first modeled using 5 precomputed SEDs based on SFHs with constant star formation rates from:

- 0.0 to 0.2 Gyr prior to  $t_{\text{obs}}$ ;
- 0.2 to 0.5 Gyr prior to  $t_{\text{obs}}$ ;
- 0.5 to 1.0 Gyr prior to  $t_{\text{obs}}$ ;
- 1.0 to 2.0 Gyr prior to  $t_{\text{obs}}$ ;
- 2.0 Gyr prior to  $t_{\text{obs}}$  to  $z = 5$ ;

where  $t_{\text{obs}}$  corresponds to the object's redshift and  $z = 5$  is taken as the onset of star formation. If the data prefer, the oldest bin could also take the form of a 1 Gyr top hat starting at  $z = 5$ . Dressler et al. (2016, 2018) examine these SFHs in detail with the latter containing a thorough treatment of their quality in its Appendix.

In the fits, the above SED bases shared a common metallicity but could take independent extinctions (Calzetti et al. 2000 law). Those were estimated by replicating the stellar template four times at four different  $A_V \in 0.0, 0.5, 1.0, 2.0$  values and finding their best-fit non-negative superposition. This process enabled each stellar population to be screened by potential complex dust geometries. Global metallicities were inferred from templates spanning  $-0.6 \leq \log Z/Z_\odot \leq 0.3$  in 0.1 dex steps with a fitting prior peaked at  $Z = Z_\odot$ . As such, the predicted spectra do not capture enrichment histories (cf. Pacifici et al. 2012; Morishita et al. 2019). The predictive accuracy of these models stands despite this shortcoming (Section 3).

The spectral templates were generated using Flexible Stellar Population Synthesis (FSPS; Conroy et al. 2009) assuming default abundance patterns. When inferring the SFHs, these models—5 mass amplitudes  $\times$  4  $A_V$ s + 1 metallicity + 1 redshift + 4 emission line/blend amplitudes = 26 free parameters—were typically constrained by 7 + **~150** photometric + spectral datapoints. Redshifts were gridded in  $\Delta z = 0.005$  increments and solved for jointly with the other parameters.

Hereafter, we refer to this approach as “Technique 1.”

### 2.1.2 Technique 2 for inferring SFHs from low resolution SEDs

Subsequent to Dressler et al. (2018), all CSI spectrophotometry was refit using a new SFH inference scheme based on a library of 500  $H = 1$  stochastic tracks (Kelson 2014; Kelson et al. 2016, 2020, Abramson in preparation). The tracks comprise 200 independent increments and are agnostic to the age of the universe: the same track can be stretched to span an arbitrary  $t \in [t_0, t_{\text{obs}}]$  interval, with the absolute size of each increment in years changing with a galaxy's redshift. The fits assumed a  $t_0$  of  $z = 10$  and the star formation increment at the sample's mean redshift was 33.5 Myr.

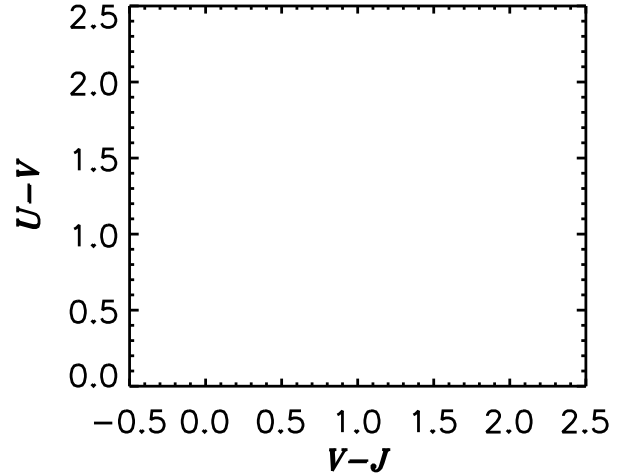


**Figure 1.** Some heuristic/contextual map of the sample data to orient the reader: UVJ plot,  $M_*$  histogram, half-mass time histogram, or all of the above. I don't want to clutter any of the subsequent plots with this stuff.

Model spectrophotometry was generated at  $\Delta z = 0.01$  intervals for redshift estimation.

These models assume monolithic values for both metallicity and extinction. Templates were generated at  $-1.5 \leq \log Z/Z_\odot \leq 0.3$  in 0.3 dex steps **with a fitting prior peaked at  $Z = Z_\odot$** . Following Pacifici et al. 2012, the fitter finds for each  $H = 1$  track in the library the probability that it generated an observed SED given a redshift, metallicity,  $A_V$ , spectral fluxing function ( $\propto \lambda^k$ ), and set of four emission line/blend amplitudes. All SED templates were generated using FSPS with default abundances.

Hereafter, we refer to this approach as “Technique 2.”

## 2.2 High resolution spectroscopy

Dressler et al. (2016, 2018) identified a class of galaxies inferred to have formed at least half of their stars within 1–2 Gyr of the epoch of observation—“late bloomers.” We obtained high resolution— $R \sim 800$ —rest-optical spectra with Magellan-IMACS to cross-check and further interpret the nature of such objects. We use these data here as the benchmarks against which to compare the predictions from the fits discussed in the previous section.

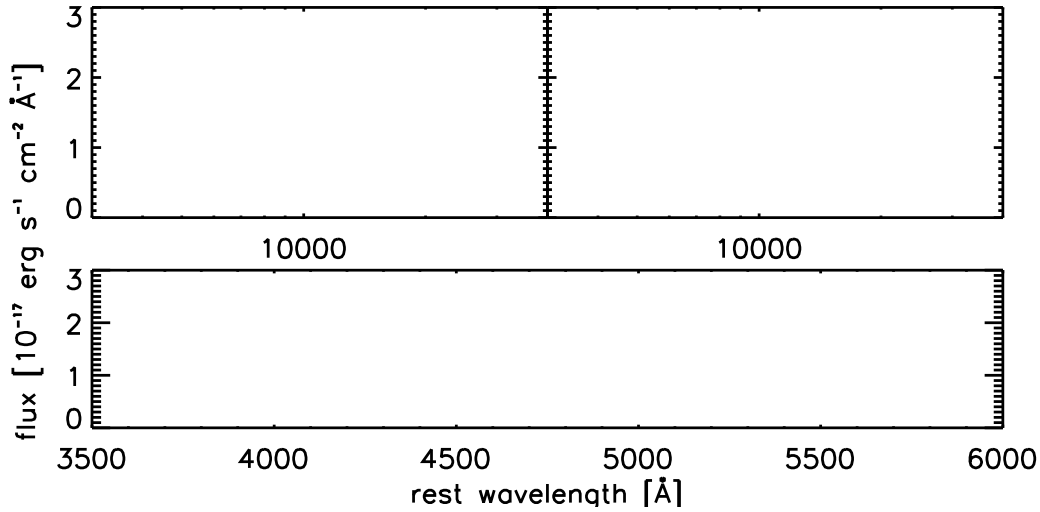
**We got the data in DATES. Here's how many objects, and a brief description of the data's S/N/quality/etc.**

Figure 1 shows the distributions in **stellar mass, UVJ colour-colour space, and inferred half-mass time** of the sample objects.

## 3 RESULTS

Here we compare the model high resolution spectra generated from the SFHs inferred using Techniques 1 and 2 (Sections 2.1.1, 2.1.2) to actual high resolution spectra taken for the same objects. In all but one case, we find that the median predicted line strength is within 1% of the measured value.

We study the model spectrum corresponding to the maximum-likelihood SFH fit. Uncertainties are tabulated for the SFHs and attendant parameters, but not propagated to the high resolution spectral models. As such, the comparisons below treat the predictions as more credible than they are. Combined with the fact that the model metallicities are age-independent, our experiment is biased towards



**Figure 2.** A 3-panel figure—2 top + 1 bottom. At top, show D18-like figures of the CSI data + SFH reconstructions for one object. I don’t think we need to show the spectral sub-components for the chunky fit; just the best fit low-res SED and SFH. Other parameters at Dan’s discretion, but they shouldn’t clutter anything up; the key is the low-res SED. At bottom, show the full IMACS high-res spectrum for the same object and overlay the matched-resolution predictions from both SFH reconstruction techniques. Whatever colors we use here we’ll stick with for the rest of the paper. The object probably should be like SA-type; nice absorption, some emission.

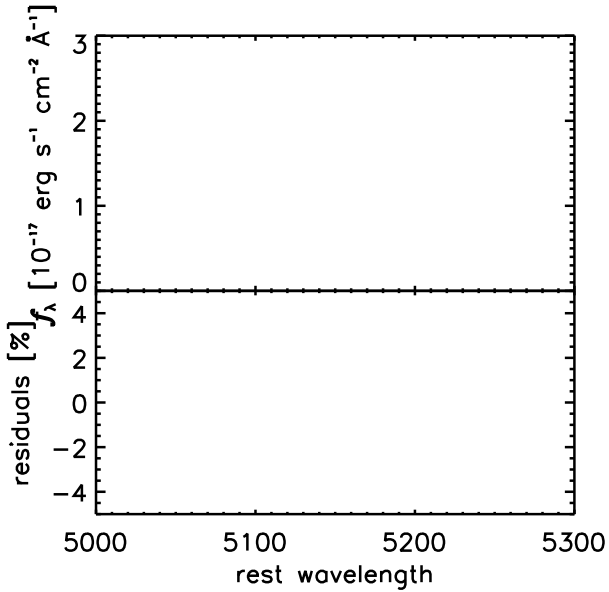


**Figure 3.** A graphic example of how we calculate whatever residuals we illustrate in Figure 4. Could be 2 panels, one showing the raw line + model, another showing the residuals. Could be 1 panel split in half. Could be for one object, or the full sample with the average models overlaid. Can just pick one SFH technique.

revealing significant differences between the data and the predictions. Any offsets we find—in units of flux or standard deviations— are thus closer to upper limits.

LEA – some note here about whether we’re going to focus on the full spectrum or just the “line strengths.” The latter is justified because it’s the real value-add of the high-res data, and also because I assume the same photometry was used to flux both the prism data and the high-res spectra. We just have to explain it.

### 3.1 Experimental setup

Figure 2 outlines the experiment. The **top** panels show the CSI spectrophotometry for a galaxy at redshift **ZZZ**, along with its inferred SFH using Technique 1 (left) and 2 (right). The CSI data have broad wavelength coverage and dense but coarse sampling over the rest optical. As such, they reflect a relatively complete accounting of a galaxy’s stellar photospheric continuum emission. With the exception of the strongest/broadest absorption features—e.g.,  $H\beta$ ; the  $Mg \lambda 5170$  triplet—these data are insensitive to absorption lines and any historical information they might convey.

Figure 2, **bottom**, shows the complete high resolution IMACS spectrum of this object with the matched-resolution spectral predictions from the SFHs in the top panels overlaid. Results from Techniques 1 and 2 are in **color 1** and **color 2**, respectively.

The data in the two top panels are identical; only the models change from left to right. Likewise, both model predictions are compared to the same  $R \sim 800$  IMACS data. We therefore perform two experiments in parallel, identical except for the method from which the high resolution prediction is generated. **We comment on the differences between the results from each technique in Sections XYZ, but they are ancillary to our main point.**

Figure 3 illustrates how we compare our spectral predictions to the high resolution data. Here, we re-present Figure 2, bottom, zoomed-in to the region surrounding **FEATURE**. LEA – If we need to divide the data by the model, we’ll make this 2 panels. The central bandpass of the corresponding Lick index is shown in **however (CITE)**. We define the mismatch between prediction and high resolution data as:

$$\Delta = \text{whatever Dan says.} \quad (1)$$

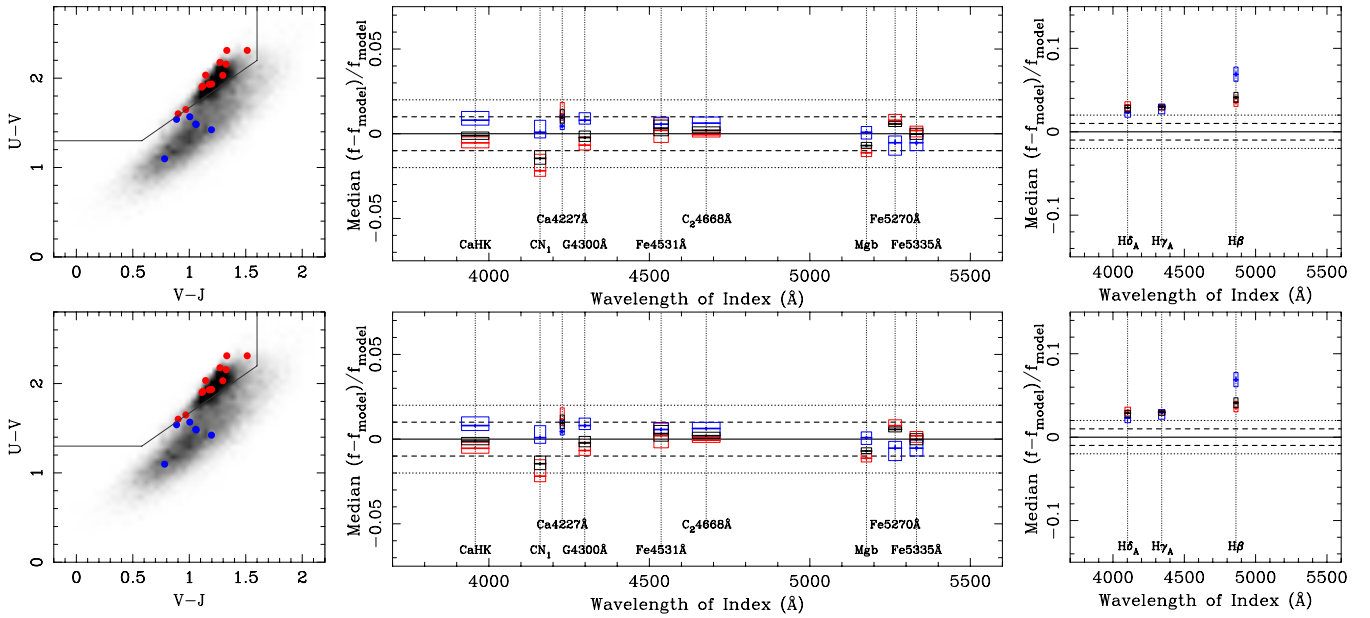
That is, a quoted difference of 5% in a given spectral feature corresponds to **whatever per-angstrom offset integrated over however many angstroms, or whatever Dan did.**

We then compute  $\Delta$  for each Lick bandpass in each galaxy.

LEA – Here is where we talk about limiting ourselves to a

**Table 1.** Summary of experimental results. Mean equivalent widths are quoted for the full sample. **Asterisks denote feature outside the CSI prism wavelength coverage.**

Feature	Band center [ $\text{\AA}$ ]	Bandwidth [ $\text{\AA}$ ]	$\langle \text{EW} \rangle$ [ $\text{\AA}$ ]	Full sample offset [%]		<b>Red</b> sample offset [%]		<b>Blue</b> sample offset [%]	
				Tech. 1	Tech. 2	Tech. 1	Tech. 2	Tech. 1	Tech. 2
CaHK	<b>LAMBDA</b>	<b>LAMBDA</b>							
CN <sub>1</sub>	4159	35	foo	foo	foo	foo	foo	foo	foo
Ca4227	4228	12							
G4300	4298	35							
Fe4531	4536	45							
C <sub>2</sub> 4668	4677	86							
Mgb	5176	32							
Fe5270	5265	40							
Fe5335	5332	40							
H $\delta$ <sub>A</sub>	4102	38							
H $\gamma$ <sub>A</sub>	4341	43							
H $\beta$	4862	28							

**Figure 4.** Main plot, only the absorption features (no Balmer), Technique 1 at top and 2 below. I think we should look at versions highlighting any ranges outside the prism bandpass (at the median or  $N$ th percentile redshift or whatever) and also see what happens when the individual residuals are lightly traced in grey or something. We also need to determine how we'll split the data (UVJ or (N)LB); if we go w/ UVJ perhaps we can add the LB/NLB version in an Appendix. I think we should also shrink the vertical scale to  $\pm 5\%$ .

comparison in the lines or mention that we calculate global  $\chi^2$  values and point to where we'll discuss those.

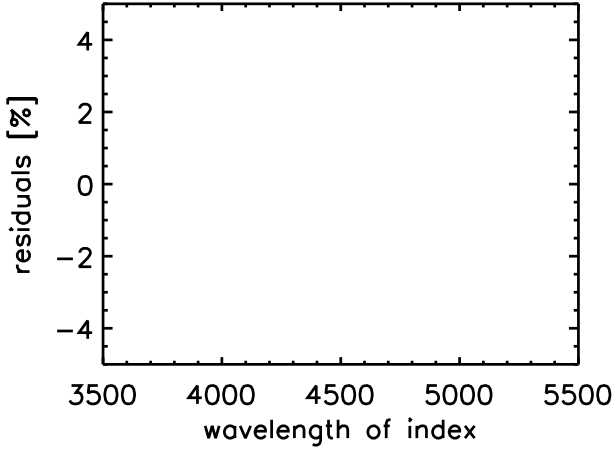
### 3.2 Sample-wide outcomes

Figure 4 and Table 1 summarize the quality of our model predictions across the entire **XXX** object sample; i.e., the overall outcome of our experiment. In the figure, results from Techniques 1 and 2 are shown in the top and bottom panels, respectively. At the central wavelength of each feature, we show the median, 16th, and 84th percentile offsets in a given sample. Results based on the full sample are shown in black, with red and blue boxes denoting **SFR-defined** subsamples, respectively. The width of each box corresponds to the width of that feature's Lick bandpass. Regimes outside the original prism wavelength range are highlighted in some

**color**. The dashed and dotted horizontal lines respectively benchmark mismatches at the  $\pm 1\%$  and  $\pm 2\%$  level.

Clearly, *almost all rest-optical galaxy absorption features visible at  $R \sim 800$  are predictable to better than 1% by models tuned to data with  $\sim 30\times$  lower resolution but broader wavelength coverage*. That is, to a very high degree of accuracy, one can infer the strengths of nearly all major optical stellar absorption features in integrated galaxy light without ever detecting any of them.

This statement holds for any feature in any subsample except one. **State mean total offsets for both types (Table 1)**. It holds irrespective of the feature's width—**basic quantification**—and irrespective of the chemical species traced. It holds for strong features—e.g., the G band in passive objects **quote mean EW**—and weak ones—e.g., Mgb in starforming ones **quote mean EW**.



**Figure 5.** Show the offsets for the Balmer line predictions; same styling as Figure 4. Can potentially add another panel for, e.g.,  $H\beta$  specifically showing the unmodelled emission. Can also put this up in Figure 3, but I think best to bury it down here.

Simply: we knew the fluxes of each Ångstrom of our high resolution spectra before we got to the telescope.

The lone exception is Ca4227 in **passive**, but not starforming galaxies. **Something about the history of this line being anomalous, Ca-rich supernovae, etc.** As CSI was designed to probe spatial overdensities, **and some of these objects are for real in dense places?**, we believe the  $\sim 2.5\%$  mismatch we see here may reflect the same phenomenon. Regardless, this finding suggests either that slightly different abundance patterns should be assumed when fitting passive objects (**CITE**), or that Ca4227 strengths might be used to enhance SFH estimates. We touch on the latter in Section 4, but note here that any prior would have to be accurate to better than 2% in the mean for this relationship to be useful.

### 3.3 The Balmer lines

Figure 5 shows the same offset summaries as Figure 4 but for the three strong Balmer lines in the prism data:  $H\delta$ ,  $H\gamma$ , and  $H\beta$ . **LEA – we’ll have to see what these look like. I don’t think there’s anything interesting to be said here, just to show that the only sizeable discrepancies are readily attributable to emission. If it holds up, we can also make a note about the enhanced performance of the  $H = 1$  models here versus the chunky fits.**

### 3.4 Systematic errors

The above comparisons are affected by **three** main systematics: redshift refinement, velocity broadening, and continuum matching.

Regarding redshift refinement, both SFH inference techniques adopted discrete redshift steps of  $0.005 \leq \Delta z \leq 0.01$  (Section 2). This interval was sufficient given the low resolution of the CSI data, but the newer IMACS data allow for more precision. As such, there are typically mismatches of  $\delta z \approx ZZZ$  between the predicted locations of spectral features and where they ultimately appear in the high resolution data.

Regarding velocity broadening, the CSI data are likewise too coarse to permit velocity dispersion estimates. As such, the high resolution spectral predictions must be broadened from the native

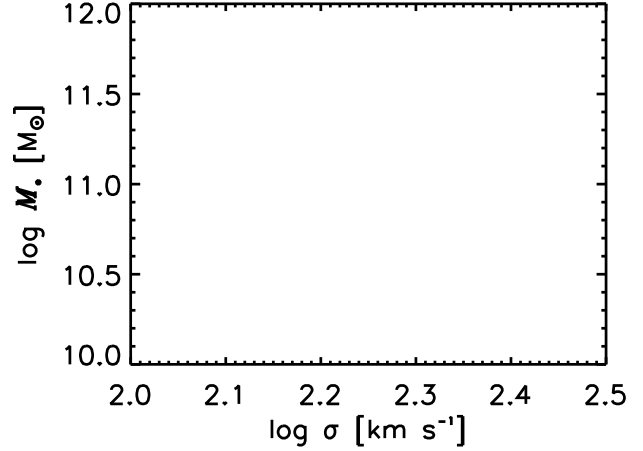


**Figure 6.** Show  $\sigma$  distributions or  $\sigma-M_*$  for LB/NLB objects.

FSPS resolution to whatever the  $R \sim 800$  IMACS data imply for each object.

We correct for both issues by **Dan to discuss how he shifts and broadens the models here.**

These offsets are important: they illustrate the only first-order orthogonal axes in the problem of SFH reconstruction: velocity and age. They also show us that higher resolution spectra add meaningful signal in Doppler—if not age—space. Unfortunately, it appears unlikely that independent Doppler information can be exploited to enhance SFH estimates (Section 4), but it is nevertheless where having high resolution data is obviously helpful.

The last systematic is mismatches in the stellar continuum. **Dan to send methods.**

## 4 DISCUSSION

### 4.1 Implications for direct SFH inference

Our experiments imply that high resolution optical spectroscopy of any quality reasonable to expect for individual distant objects will not meaningfully enhance knowledge of their underlying stellar populations compared to much more coarsely and broadly sampled datasets (see Section 4.1.4). That is, absorption line details—at least as presented at a galaxy’s velocity dispersion—are sufficiently correlated to stellar continua on large scales that capturing the details of the latter across a long enough wavelength baseline yields the same information as densely sampling the rest optical. There is therefore no need to obtain costly, high resolution spectroscopy for SFH inferences.<sup>1</sup> **In this, we reinforce findings by Pacifici et al. (2012), who show that—limited to rest optical data— $R \sim 1000$  spectra enhance SFH estimates less than other inferences compared  $R \sim 100$  spectra (25% v. 45% drops in uncertainty; see their Table 2).** We would add, however, that, had that study incorporated UV–IR photometry, those gains would have been reduced. **LEA – (Leja et al. 2019; Lower et al. 2020) show that once you have the kind of coverage we have changing the SFH parameters**

<sup>1</sup> A future paper will show that, at  $z \sim 0.4$ , the 26-band UltraVista filter set (Muzzin et al. 2013) performs similarly to CSI, meaning that even the prism data used here is likely oversampled.



modulate the high resolution spectra at the 1%–2% level. Further insights into galaxy growth will not be gleaned by adding better spectra, but rather from the methods and results that reveal why that statement is true.

This lesson is not new. The fact that metallicity modulates continuum light on  $\sim 100\text{--}1000\text{ \AA}$  scales is apparent in the output of any stellar population synthesis code. The phenomenon is also well recognized in some contexts, such as as the tracking of Balmer line depths with  $U - B$  or D4000 (e.g., [Kauffmann et al. 2003](#); [Cid Fernandes et al. 2005](#)). What we have shown is simply that the above is true—perhaps to a greater than expected extent—for all (Lick) species. The observational trick is to sample the SED so as to capture all of the relevant signal at minimal cost. We do not know the optimal sampling, only that CSI apparently meets the criteria that define it.

Nevertheless, these findings reinforce or suggest practical, informatic, and theoretical programs that we believe will be more informative than simply taking more or “better” data.

#### 4.1.1 Practical

The practical upshot of the above is twofold. First, there is no need to expend telescope or computer time obtaining and modeling thousands of SED points for the purpose of inferring galaxy growth. Second, on the modeling side, the physical correlations between spectral elements should be accounted for mathematically to avoid drawing inferences of unreasonable certainty. Each pixel may be formally independent, but it does not add a new degree of freedom. LEA – this is the place to discuss previous work on or findings to this effect. The fact that  $S/N$  doesn’t really matter has been noted in a bunch of places before, e.g., [Leja et al. \(2019\)](#). We disagree with those authors about the utility of adding bedder spectra—even though they see similar offsets to us (2%; their Figure 8)—but may agree with [Ocvirk et al. \(2006\)](#) about it?

The narrative here is something like: limited to the rest optical, [Pacifi](#) showed there’s only marginal gains from going to  $R=1000$  spectra for SFH inferences vs  $R=100$ . [Leja](#) showed that, using UV–IR photometry,  $S/N$  doesn’t matter for SFH inferences. We do something like combine the two: if you have sufficiently broad SED sampling, the SFHs you infer are good enough to remove any reason for  $S/N$  or resolution to matter because all of the information those things could add has been accounted for.

Also, we’re working at about 1/2 the age of the universe at least compared to [Camilla](#), if not [Leja](#), too.

#### 4.1.2 Informatic

The informatic upshot of the above is that there exists a data compression scheme—a way to distill covariant pixels to independent degrees of freedom—that may be worth identifying if SFH inferences for large samples is to play a substantial role in extragalactic astronomy’s future. Given the deluge of SEDs that PFS, LSST, and WFIRST will soon deliver, modeling efficiency will be critical to characterising representative swaths of those datasets. It is likely that such a compression scheme will resemble what intuition and, e.g., CSI suggests: sparse UV and IR sampling with finer—but not fine—sampling over the rest optical, particularly from around the Balmer break to around the magnesium triplet, where intermediate age stars make the greatest impression (e.g., [Dressler et al. 2016](#)). However, it is also possible it will not resemble that configuration, so we encourage serious work on this issue (or cite and amplify).

#### 4.1.3 Theoretical

The theoretical upshot is that understanding this compression scheme—even if it is as basic as the above—represents understanding the extent to which information about the physics an object was subject to over its history could possibly modulate its presentation at the one epoch we will ever witness it at. That is, it must reveal the bedrock of the SFH  $\mapsto$  SED mapping, and therefore something close to the epistemological ceiling for the study of galaxy evolution. Knowledge of that boundary condition cannot but enhance the questions investigators ask and the investigations they pursue. Given the substantial human and technological resources devoted to such endeavors, that insight seems beneficial.

How mechanically to reverse engineer this compression scheme is a separate question. Machine learning could be used to identify via simulation the hypersurface characterising the precision to which  $M_*(t)$  is knowable as a function of data— $S/N$ , SED sampling—and galaxy properties— $z$ , sSFR,  $Z$ ,  $\sigma$ ,  $A_V$ , environment, morphology. A simpler exercise, is simply to invert the experiment we performed, fitting SFHs only to high resolution optical spectra and predicting broadband fluxes the blue and red. One could then repeat this exercise downgrading the resolution or omitting portions of the starting spectrum and measuring how the extrapolations changed, adding outtrigger photometry as soon as the predictions began to deviate significantly from the truth. Figures 12 and D2 of [Abramson et al. \(2020\)](#) show an examples of this kind of approach—and hint at the predictive quality as a function of SED type—which of course could also be coupled to machine learning.

Based on our results, however, similar exercises performed using only photometry ([Abramson](#) in preparation), and the physics at play, we suspect that full UV–IR wavelength coverage will be one of the foundations whatever map is finally produced: If all of the starlight is captured, the density of the sampling is secondary (provided it is sufficient to obtain accurate redshifts). Future surveys designed to support SFH reconstruction should therefore opt for increased wavelength coverage at the expense of SED resolution.

Of course, we are not asserting that there is never a reason to take high resolution spectra. If one is interested in the IMF ([Conroy & van Dokkum 2012](#)), specific abundance patterns, or kinematics, it is clearly necessary. We only argue that it seems very unlikely that these investigations will qualitatively enhance assessments of galaxy growth.

The only avenue we have found where they might is calcium strengths. These seem to add a relatively large amount of information to our predictions in passive galaxies compared to the other Lick indices. However, while the prediction/data mismatches are indeed twice the average offset, they are still only at the 2% level. As such, to enhance SFH predictions, priors linking Ca abundance to age must be accurate to at least that level, and spectra must have  $S/N \gtrsim 14\text{ \AA}^{-1}$  to see the signal at  $1\sigma$ . We believe attempting to construct such an object or take such data are endeavors of diminishing returns: aperture and other observational effects surely distort one’s ability to interpret such precision when present, and—as in the case of calcium—other, more easily observed properties like environmental density (CITE) are almost certainly equally good candidates for an age prior.

#### 4.1.4 What about stacking?

If  $\sim 1\text{--}2\%$  line strength precision is unobtainable for useful numbers of individual objects, it can be achieved through stacking (CITE). In principle, modeling the stacks could reveal the growth

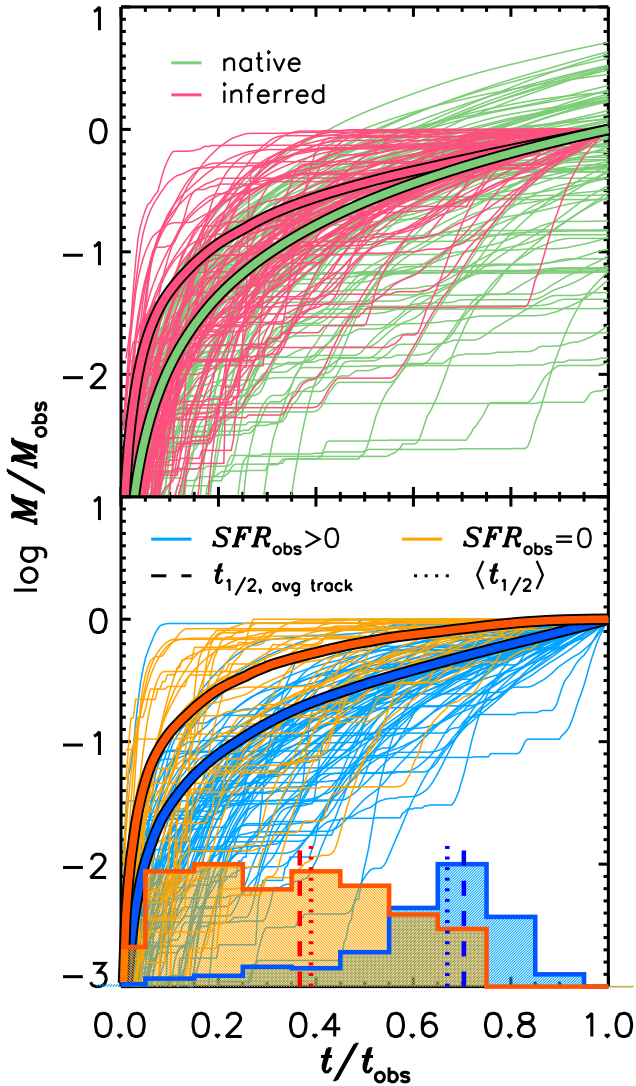


**Figure 7.** LEA – here’s why stacking will not buy you much. The difference between the various half mass time averages is  $\sim 2\%$ – $3\%$ . I’m not sure if that matters but I calculated it.

trajectory of the average constituent object. This statement is mathematically true, but physically unhelpful.

Figure 7 explores different kinds of  $H = 1$  math growth histories, the prior behind our Technique 2 SFH inferences (Section 2.1.2). These tracks are similar to, e.g., the suite of semi-analytic model-derived histories used by Pacifici et al. (2012).

The top panel shows the native distribution of  $H = 1$  trajectories modeled forward from  $t = 0$  to  $t = 1 = t_{\text{obs}}$  in green, with the ensemble’s mean mass normalized to  $\langle M \rangle = 1$  at  $t_{\text{obs}}$ . The same distribution of tracks is overlaid in pink but normalized such that each track has  $M(t_{\text{obs}}) = 1$ . The latter go into the fitting, with the luminosity and color of any object confining each track in the library to a small range of normalizations.

Note that the inferred mean histories of these two suits are different, even though they are the same tracks. Stepping forward, as the galaxies do, is different than stepping backwards, as the fitter does (see also Behroozi et al. 2013; Torrey et al. 2017). It is the difference between mean histories that must be inferred to assess whether  $H = 1$  stochasticity provides a physically accurate is the

correct SFH reference set. As this difference is (a) large, and (b) derived from a stack of histories, not good precision on single tracks, high precision data are not needed. LEA – I think I’m gonna cut this.

The bottom panel shows a more intuitive example. We reproduce the pink tracks from the top panel split into those that lead to passive (orange) or starforming (blue) galaxies at the epoch of observation. The half-mass time distributions for each subsample are shown at the bottom. From only these, it is clear that a stack based on objects of the same stellar mass and SFR—intuitive bins to construct—might contain objects with half-mass times that differ by 40% of a Hubble time. What the average of these tracks—at any precision—says about the physics causing any one of them to behave as it did is hard to see.

The fundamental issue is that there are only two objects of physical interest: (1) high-fidelity assessments of individual SFHs, or (2) the typical SFH of a meaningfully defined class of galaxies. Due to  $S/N$  requirements, (1) is not obtainable. Meanwhile, (2) is an average over histories, and so is certainly assessable by combining many low-fidelity inferences for individual objects, which don’t require good data.<sup>2</sup>

Of course, whether a meaningful class of objects is compilable from observed properties is questionable, and certainly require parameters beyond what are shown in Figure 7, bottom. If you can, however, the physical inference may ultimately be in the difference between forward and backward projected SFH inferences (top).

For neither purpose are high-precision, high-resolution spectra beneficial. LEA – basically, the physics is in the histories (if anywhere), so you want to stack the histories (if anything), and for that you don’t need good data at the single object level. Maybe there’s room to compare the stack of histories to the history derived from a stack? What would that tell you? Something about loss-of-signal lookback horizons?

## 4.2 Prospects for exploiting Doppler information

The area where high resolution spectroscopy yields unique insight is velocity space. The obvious enhancement is to redshifts. This may be important to mitigate against, e.g., [O II] emission masquerading as an enhanced Balmer break at low resolution, biasing galaxy ages toward those of A stars. However, a more potentially useful application for SFH reconstruction is through using kinematics inferred from line profiles.

It’s tempting to contemplate using velocity dispersions to place colour-independent total stellar mass priors on SED fits to data of any resolution. This move is especially appealing because it would provide a handle on faint/old stars that might imprint on a galaxy’s velocity dispersion but remain undetectable in its SED. Unfortunately, a number of complications suggest that doing so would not significantly improve current methods.

The prior would most readily enter through a  $\sigma$ – $M_*$  relation. The intrinsic scatter of this relation is  $\sim 0.2$  dex (CITE), much broader than the formal—or even systematic—errors on SED-inferred stellar masses (quote what we find; systematics as cross-method or duplicate obs differences). Further, that relation would

<sup>2</sup> It is actually not clear that (2) is obtainable, either. “Typical” in this context should properly refer to the mode history; that which describes the largest fraction of class members. It may be that the mean history is our only proxy for this, but it is not in reality the object of interest.

be calibrated to stellar masses suffering the same systematic errors one wishes to correct by using the relation. Theoretically, a  $\sigma$ –Sérsic index–color relation—or some equivalent structure—could be used, but this entails other issues regarding spatial resolution, aperture matching, and dust effects. Finally, due, e.g., to inside-out growth (CITE) and the existence of thick disks, each stellar subpopulation may contribute its own velocity dispersion to the global profile. If so, modeling dispersions will re-introduce exactly that the same degeneracies in line decomposition as arose with SEDs. These effects would have to be marginalized over—negating the precision gains—or the systematics from failing to do so would have to be understood.

**UTILITY AFTER SELECTION BY SFH**—Figure 6 illustrates the sample’s velocity dispersion estimates. Here, we show **what we show** for galaxies split by their inferred growth histories. **LBs show behavior X while NLBs show behavior Y.** needed to say for certain, these trends suggest a link

We are bearish on the ultimate utility of kinematic stellar mass constraints, but we also do not know of any SFH modeling that has attempted to incorporate it. A study assessing its practicality and real-world effects would be edifying.

**NIRSPEC no good for SFHs but ok for kinematics + environments. Cosmology.**

## 5 SUMMARY

In the context of SFH reconstruction from full spectral fitting: high resolution doesn’t buy you anything new.

- You can predict line strengths to 1% without measuring them.
- Wavelength coverage beats spectral resolution.
- Metal enrichment histories for at least our sample are consistent with flat to whatever corresponds to 1% differences in line strengths.
- The goal is not to fit SFHs to SEDs, but to understand the sampling/compression scheme that enabled us to find what we found. This is the SFH→SED mapping and is equivalent to understanding the epistemological ceiling in the study of galaxy evolution.

*Facilities:* Magellan/IMACS

*Software:* Python (CarPy).

## ACKNOWLEDGEMENTS

LEA thanks Dr. Lindsay Young for allowing him to find a place to write this text.

## REFERENCES

- Abramson L. E., Brammer G. B., Schmidt K. B., Treu T., Morishita T., Wang X., Vulcani B., Henry A., 2020, *MNRAS*,  
 Behroozi P. S., Marchesini D., Wechsler R. H., Muzzin A., Papovich C., Stefanon M., 2013, *ApJ*, **777**, L10  
 Calzetti D., Armus L., Bohlin R. C., Kinney A. L., Koornneef J., Storchi-Bergmann T., 2000, *ApJ*, **533**, 682  
 Chabrier G., 2003, *PASP*, **115**, 763  
 Cid Fernandes R., Mateus A., Sodré L., Stasińska G., Gomes J. M., 2005, *MNRAS*, **358**, 363  
 Conroy C., van Dokkum P., 2012, *ApJ*, **747**, 69  
 Conroy C., Gunn J. E., White M., 2009, *ApJ*, **699**, 486  
 Dressler A., et al., 2016, *ApJ*, **833**, 251  
 Dressler A., Kelson D. D., Abramson L. E., 2018, *ApJ*, **869**, 152

- Kauffmann G., et al., 2003, *MNRAS*, **341**, 33  
 Kelson D. D., 2014, preprint, ([arXiv:1406.5191](https://arxiv.org/abs/1406.5191))  
 Kelson D. D., et al., 2014, *ApJ*, **783**, 110  
 Kelson D. D., Benson A. J., Abramson L. E., 2016, preprint, ([arXiv:1610.06566](https://arxiv.org/abs/1610.06566))  
 Kelson D. D., et al., 2020, *MNRAS*, **494**, 2628  
 Leja J., Carnall A. C., Johnson B. D., Conroy C., Speagle J. S., 2019, *ApJ*, **876**, 3  
 Lower S., Narayanan D., Leja J., Johnson B. D., Conroy C., Davé R., 2020, arXiv e-prints, [p. arXiv:2006.03599](https://arxiv.org/abs/2006.03599)  
 Morishita T., et al., 2019, *ApJ*, **877**, 141  
 Muzzin A., et al., 2013, *ApJ*, **777**, 18  
 Ocvirk P., Pichon C., Lançon A., Thiébaud E., 2006, *MNRAS*, **365**, 46  
 Pacifici C., Charlot S., Blaizot J., Brinchmann J., 2012, *MNRAS*, **421**, 2002  
 Torrey P., Wellons S., Ma C.-P., Hopkins P. F., Vogelsberger M., 2017, *MNRAS*, **467**, 4872  
 Worthey G., 1994, *ApJS*, **95**, 107  
 York D. G., et al., 2000, *AJ*, **120**, 1579

This paper has been typeset from a  $\text{\LaTeX}$  file prepared by the author.